Shell properties and concentration stability of acoustofluidic delivery agents

Hussain Alsadiq[a, *], Karnaker Tupally[b], Robert Vogel[c], Ganesh Kokil[b], Harendra S Parekh[b], Martin Veidt[a]

[a]School of Mechanical and Mining Engineering, University of Queensland, Brisbane, Australia

[b]School of Pharmacy, University of Queensland, Brisbane, Australia

[c]School of Mathematics and Physics, University of Queensland, Brisbane, Australia

Abstract- This paper investigates the shell elastic properties and the number-concentration stability of a new acoustofluidic delivery agent liposome in comparison to Definity™, a monolayer ultrasonic contrast agent microbubble. The frequency dependent attenuation of an acoustic beam passing through a microbubble suspension was measured to estimate the shell parameters. The excitation voltage was adjusted to ensure constant acoustic pressure at all frequencies. The pressure was kept at the lowest possible magnitude to ensure that effects from nonlinear bubble behaviour which are not considered in the analytical model were minimal. The acoustofluidic delivery agent shell stiffness S_p and friction S_f parameters were determined as ($S_p = 0.11$ N/m, $S_f = 0.31 \times 10^{-6}$ Kg/s at 25 °C) in comparison to the Definity™ monolayer ultrasound contrast agent which were ($S_p = 1.53$ N/m, $S_f = 1.51 \times 10^{-6}$ Kg/s at 25 °C). When the temperature was raised to physiological levels, the friction coefficient S_f decreased by 28% for the monolayer microbubbles and by only 9% for the liposomes. The stiffness parameter S_p of the monolayer microbubble decreased by 23% while the stiffness parameter of the liposome increased by a similar margin (27%) when the temperature was raised to 37 °C. The size distribution of the bubbles was measured using Tenable Resistive Pulse Sensing (TRPS) for freshly prepared microbubbles and for bubble solutions at 6 hours and 24 hours after activation to investigate their number-concentration stability profile. The liposome maintained > 80% of their number-concentration for 24 hours at physiological temperature, while the monolayer microbubbles maintained only 27% of their number-concentration over the same period. These results are important input parameters for the design of effective acoustofluidic delivery systems using the new liposomes.

Keywords: acoustic attenuation, acoustofluidics, ultrasound contrast agent, liposome.

* Corresponding Author: Hussain Alsadiq, School of Mechanical and Mining Engineering, The University of Queensland, St Lucia, Qld, 4072, Australia. Email: h.alsadiq@uq.edu.au , Phone: +61 405495660.

INTRODUCTION

The use of biodegradable microbubbles as diagnostic ultrasonic contrast agents (UCA) in enhancing clinical sonography has proven an efficient and safe tool for human application over many decades [1]. There have been several studies on their production and chemical composition [2], shell and acoustic properties [3,4], and this has extended into evaluation of their potential as drug delivery systems [5,6]. They have been clinically approved for diagnostic application, such as enhancing the ultrasonic imaging of the left ventricle for decades. The use of microbubbles for theranostic applications has been proposed in several studies [7-9], however there is limited understanding of their performance under simulated physiological conditions.

The concepts proposed for microbubbles in drug delivery applications can be classified into three categories: 1) microbubble-induced sonoporation, to enhance cell/tissue membrane permeability, where bubbles are co-administered with bioactive substances as separate entities [10-13]; 2) microbubbles with the bioactive substance attached to the surface of the shell through electrostatic attraction or covalent attachment [14], and 3) microbubbles encapsulating bioactive substances in their core [15]. The latter not only protects untargeted organs from being exposed to the bioactive substance which could elicit unwanted side effects, but also protects the bioactive substance from degradation and shields it from the body's immune system [9].

A new fabrication process, generating highly stable nano-size echogenic liposomes (ELIP) designed as acoustofluidic delivery agents has shown extended number-concentration and echogenic stability [8,16]. Preliminary investigations using an *ex vivo* bovine eye model have also shown that it has enhanced acoustofluidic properties for intravitreal drug delivery to the posterior eye [17]. The same fabrication process, when used to produce microbubbles has also been shown to maintain 91% of its number-concentration for 24 hours at 25 °C [18]. The radius-dependent zeta potential of the formulation has also been studied for varying lipid compositions using Tuneable Resistive Pulse Sensing (TRPS) [19]. The latter study showed that varying the lipid composition (dipalmitoylphosphatidylcholine (DSPC) to 1,2-dimyristoyl-sn-glycero-3-phosphoglycerol(DMPG)) ratio impacted its zeta potential. The relative increase of the negatively charged lipid, DMPG over the neutral lipid, DSPC ratio resulted in overall lowering of zeta potential which indicated that ELIP with desired, zeta-potential can be formulated.

This body of work now extends into detailed investigation of shell properties and number-concentration stability profile of the aforementioned acoustofluidic delivery agent, comparing this to a commercially available monolayer microbubble diagnostic contrast agent, Definity™. The investigation of the shell parameters of the delivery agent is a prerequisite to studying their acoustofluidic behaviour, as shell parameters are crucial inputs in models used to predict the microbubbles' translation velocity arising from sonication [20]. An important feature of the frequency-dependent attenuation measurements in this study is that they have been performed at constant pressure to eliminate pressure-dependent attenuation effects, and at the lowest possible pressure levels to avoid influences from large, nonlinear bubble deformations.

Size measurements presented in this study were performed using Tunable Resistive Pulse Sensing (TRPS), in comparison to other studies that use coulter counter technique. This allowed detection of microbubbles with diameters as small as 200 nm, and therefore a more accurate measurement of the size distribution and concentration. The methodology used is a significant improvement to previous studies that used coulter counter techniques with minimum measurable diameter of 0.46 μm [21] and 0.6 μm [22]. The size of the MBs directly affect frequency attenuation curves [21] and size and concentration measurements affect the shell parameters estimations. Furthermore, accurate measurements of MBs and ELIPs size distributions and concentrations are crucial for drug delivery applications as they are directly related to the dosage of the drug loaded in the population of the agents.

In the background section, theoretical models used to analyse the measurements are presented together with the crucial assumptions used to derive them. In addition, results of previously reported shell properties of Definity™ microbubbles are summarised and critically discussed. The materials, experimental setups and procedures used in this study are then presented in the methodology section. The findings of the study are presented and analysed in the results and discussion sections. Finally, concluding remarks and recommendations for future work are presented in the conclusion section.

BACKGROUND

The measurement of frequency dependent attenuation factor of acoustic wave through microbubbles solution can be used to estimate the shell properties, utilizing the acoustic model of shell-stabilized microbubbles which is described in detail in [23].Attenuation measurements can be obtained by measuring the transmission loss of an acoustic wave through a suspension of microbubbles. The attenuation factor $\alpha(r,f)$ of microbubbles of radius r at frequency f is found as:

$$\alpha(r,f) = \frac{10}{\ln(10)} * \sum_{r} n(r) * \sigma_s(r,f) * \frac{\delta_{tot}}{\delta_{rad}} \quad (1)$$

where $n(r)$ is the number density of the microbubbles that can be obtained by any particle counting technique, δ_{tot} is the total damping, $\delta_{rad}$is damping due to radiation, and $\sigma_s(r,f)$ is the scattering cross-section shown by Medwin [24] to be:

$$\sigma_s(r,f) = \frac{4\pi r^2}{\left\{\left(\frac{f_0(r)}{f}\right)^2 - 1\right\}^2 + \delta_{tot}^2(r,f)} \quad (2)$$

where $f_0(r)$ is the resonance frequency of a bubble of particular radius.

The total damping δ_{tot} can be approximated as the summation of damping due to radiation δ_{rad} , viscosity δ_{vis} and shell friction δ_{sh} such as:

$$\delta_{rad} = \frac{\omega R}{c} \quad (3) \qquad \delta_{vis} = \frac{4\eta}{\omega\rho R^2} \quad (4) \qquad \delta_{sh} = \frac{S_f}{4\pi\omega\rho R^3} \quad (5)$$

Where ω is the angular frequency ($2\pi f$), c is the acoustic velocity in the liquid (1500 m/s) for water, η is the liquid viscosity (0.001 Pa.s), and S_f is the shell friction coefficient. The resonance frequency $f_0(r)$ derived considering small radial oscillation with respect to the resting radius and assuming the shell is a viscoelastic solid was found by de Jong model [25] as:

$$f_0(r) = \frac{1}{2\pi}\sqrt{\frac{3\gamma P_0}{\rho R^2} + \frac{2S_P}{\rho R^3}} \quad (7)$$

Where P_0 is the ambient pressure (101.7 kPa), γ is the polytropic exponent of the contained gas which is 1.06 for octafluoropropane used in both agents in this study, S_p is the shell stiffen coefficient, and ρ is the liquid density (1000 kg/m^3). Other models with different assumptions on the shelling medium concludes to a very similar resonance frequency equations [26].

Equation 1 can be modified as in [22] to be:

$$\alpha(r,f) = \frac{10}{\ln(10)} * N_{fit} \sum_{r} n_k(r) * \sigma_s(r,f) * \frac{\delta_{tot}}{\delta_{rad}} \quad (8)$$

where N_{fit} is the total number of bubbles per unit volume, and n_k is the normalized number distribution. In this form the value of N_{fit} is calculated from the attenuation measurement not from the size distribution measurement. This is because not all the liposomes counted in the size measurement contain gas and therefore they do not contribute to the attenuation.

Critical aspect of experimental procedure

The model described in the previous section has been used in several studies to characterise Definity™ microbubbles (Table 1). The attenuation of the pressure wave through microbubble suspensions is measured either using pulse echo or through transmission ultrasonic techniques, and the measured values are curve fitted with the

model to estimate the shell parameters S_p and S_f. Size and concentration measurements as well as the implementation strategy of the theoretical model have a significant influence on the estimated shell properties. In addition, the models described above to estimate the elastic properties of microbubble shells are based on a number of crucial assumptions: 1) the magnitude of the radial oscillation is very small relative to the resting radius [25].2) the bubbles are oscillating linearly, 3) the bubbles behave as individual entities [24] and not as clusters, and 4) the bubbles' radial response is due to the primary acoustic source, and is not influenced by other bubbles due to secondary Bjerknes force effects. These assumptions require that the bubbles have to be excited at the lowest possible acoustic pressure and that characterisation is done for highly diluted suspensions.

The shell properties calculated using frequency dependent attenuation measurement are estimations derived from polydisperse populations of microbubbles. The frequency effect on the bubbles is dependent on their size, therefore bubbles with different diameters will respond to a particular frequency with different levels of oscillations. The presence of larger bubbles contributes to higher attenuation at lower frequencies, and therefore shifts the curve to lower frequencies. As a consequence, this results in stiffness coefficients that are too low and do not accurately represent the stiffness of the smaller bubbles. Thus, the values of shell properties estimated using this technique should be interpreted with caution.

The last four rows in Table 1 show that increasing the temperature from room temperature to physiological temperature results in a lower friction coefficient estimation. The shell stiffness coefficient estimation is also decreased when the temperature is increased. This could be because of the thermal radial expansion resulting due to temperature increase, causing higher attenuation at lower frequencies which consequently will result in lower stiffness coefficient estimations. A verification of the shell properties change due to temperature change on individual bubbles could be investigated using optical acquisition of radial dynamic response due to sonication [27,28]. However, imaging small microbubbles at high frequencies and low radial oscillations is challenging. On the other hand, increasing the excitation pressure to produce higher radial oscillations can result in non-linear oscillation as explained in the next section.

Table 1: Summary of previously reported shell properties of Definity™ microbubbles

Study	$f_{(MHz)}$	$P_{(kPa)}$	T (°C)	Method	Dilution	$S_p(N/m)$	$S_f\ 10^{-6}\ (kg/s)$
[21]	13-29	$P_{pp} = 25$	room temperature	Pulse-echo (2 µm filtered)	1:15000	1.51±0.36	0.016±0.016
[21]	12-28	$P_{pp} = 25$	Room temperature	Pulse-echo	1:15000	1.71±0.24	0.015 ± 0.015
[29]	7-15	$P_{pp} = 107$	room temperature	Through transmission	1:15000	1.64±0.33	0.15±0.02
[29]	15-25	$P_{pp} = 107$	room temperature	Through transmission	1:15000	2.04 ± 0.67	0.01 ± 0.01
[30]	2-25	$P_{pp} = 30$	25	Through transmission	1:2000	1.76 ± 0.18	0.21 ± 0.07
[30]	2-25	$P_{pp} = 30$	37	Through transmission	1:2000	1.01 ± 0.07	0.04 ± 0.04
[22]	2-25	$P_{-p} = 31$ $P_{+p} = 24$	25	Through transmission	1:2000	1.76 ± 0.16	0.47 ± 0.05
[22]	2-25	$P_{-p} = 31$ $P_{+p} = 24$	37	Through transmission	1:2000	1.10 ± 0.15	0.20 ± 0.04

where P_{pp} is peak to peak pressure, P_{-p} is peak negative pressure and $P_{+p}$is peak positive pressure.

Influence of pressure-dependent attenuation

Pressure-dependent attenuation is a crucial factor that should be avoided when investigating frequency-dependent attenuation, as microbubbles have been shown to have a significant pressure dependent attenuation factor [31-33], and the model does not account for the excitation pressure level. The pressure dependent attenuation influence on the shell properties estimation is observed in (Table-1), where higher excitation pressure increases the shell stiffness estimation over approximately similar frequency ranges. The estimated shell stiffness, as reported in the pertinent studies increases from 1.71 N/m at 25 kPa to 1.76 N/m at 30 kPa and 55 kPa to 2.04 N/m at 107 kPa at room temperature, and from 1.01 N/m at 30 kPa to 1.1 N/m at 55 kPa at physiological temperature.

The pressure to excitation voltage variance is also an inevitable transducer limitation. Ultrasonic transducers are designed and manufactured to perform at certain centre frequencies, and tend to produce a lower pressure to excitation voltage ratio far from their centre frequencies. Depending on the transducer type their bandwidth could be as narrow as having -6dB drop at 1 MHz away from their centre frequency. That means with the same excitation

voltage, the transducer will produce half of the pressure it produces at its central frequency. This can dramatically change the magnitude of the measured frequency dependent attenuation data. This, in consequence has a significant effect on the shape of the calculated frequency dependent attenuation curve using the analytical model and the magnitude and frequency of its peak, which is ultimately used to calculate the shell stiffness and friction coefficients. For example, using a 2.25 MHz transducer excited with an excitation pulse centred at 1.5 MHz, gave a frequency-attenuation curve peaking at approximately 2 MHz [31], while several studies listed in (Table-1) showed the attenuation curve peaking at approximately 10 MHz. Although the study by Chen et al. was not investigating frequency dependent attenuation, it illustrates the influence of the transducer spectra on the frequency-dependent attenuation curve and the importance of performing frequency-dependent attenuation experiments at constant pressure.

In addition, the magnitude of the excitation pressure affects the mode of vibration of the microbubbles and may cause translation of microbubbles and cluster formation. Studies published earlier found that individual microbubbles sonicated at 4-13.5 MHz, can undergo nonlinear behaviours at acoustic pressures as low as 13 kPa [34] and 12.5 kPa [35] for BR-14 (Bracco S.A., Geneva, Switzerland) . The effect of pressure on the frequency dependent attenuation of the latter MBs was studied in details in [36], where higher excitation pressures were shown to produce non-linear resonance and shift the frequency dependent attenuation peak to lower frequencies. Similar trends of peak shifting to lower frequencies at higher pressures were also observed in[37] for a different phospholipid formulations. A threshold pressure of microbubbles translation was observed for single MB [38] and populations of MBs [39]. Single Definity™ microbubbles showed observable translation at 50 kPa and 1 MHz [38]. Significant movement and clustering in low dilutions (1:20) were observed under continuous sonication at pressures as low as 6 kPa at 3 MHz [39]. Therefore, preforming the frequency dependent attenuation experiments at low pressure and small number of cycles enhance the reliability of the results.

METHODOLOGY

Through transmission attenuation measurements and size distribution and concentration measurements were performed on both Definity™ and ELIP at room temperature and physiological temperature. In order to limit the variables in this study, excitation pressures were calibrated to be constant at all frequencies and the microbubbles were enclosing the same gas. The aim of the measurement on the monolayer Definity™ microbubbles was to compare the results using the optimised, constant low-pressure excitation methodology with the results of previously published studies summarised in Table 1. This section details the bubbles formulation techniques and the experimental setups and procedures.

Microbubbles preparation

For monolayer lipid microbubbles, the commercially available product Definity™ (Lantheus Medical Imaging, VIC, AU) was sourced and activated according to manufacturer instructions. Briefly, a 1.5 mL vial that contains 6.52 mg/mL of octafluoropropane gas and a blend of lipids [40] was stored at 2-8°C . To activate the vial, it was allowed to warm to 25±1 °C and then agitated at 4530 ± 100 oscillations per minute for 45 s using a VialMix® instrument (Lantheus Medical Imaging®, VIC, AU). After activation, monolayer lipid microbubbles containing octafluoropropane gas were formed.

For ELIP, a lipid blend consisting of 17.24 mg DPPC and 4.2 mg DSPE–PEG2000, 94:6 molar ratio dipalmitoylphosphatidylcholine to 1,2-distearoyl-sn-glycero-3 phosphorylethanolamine (Avanti®, Alabama, US) was prepared by dissolving the lipids in ethanol (4 mL). The solution was then transferred to a round bottom flask and the flask was connected to a rotary evaporator rotating at 150 rpm in a 60±1 °C water bath, to remove the ethanol *in vacuo*. A thin lipid film was then formed on the wall of the flask. The flask was then filled with 10 mL of phosphate buffered saline (PBS) solution and rotated for 15 minutes at 51±1 °C for rehydration. The solution of lipids and PBS was then transferred to 10 mL crim cap vials, with 5 mL of the solution pipetted into each vial. At 51±1 °C, house vacuum was applied to the vials to eliminate air, and they were then filled with 10 mL octafluoropropane gas (at atmospheric pressure). The vials were then vortexed at 1500 rpm at 60 °C for 20 minutes and snap cooled in ice to form ELIP. The vials were then stored at 2-8°C. A thorough and detailed description of the processing steps can be found in the patent application [16].

Both sets of microbubbles then underwent ultrasonic imaging to investigate their echogenicity. The microbubbles suspensions were diluted with PBS by a factor of 1:500 and transferred into a 3 mL syringe with an inner diameter of 9 mm. The syringe was then scanned using a Ultrasound-on-Chip™ probe (Butterfly IQ®, Guilford, US) at a frequency of 18 MHz and mechanical index of MI: 0.26, to verify that they have been activated properly.

Size and concentration measurements

Tunable Resistive Pulse Sensing (TRPS) technique was used to measure the size distribution and the concentration of the bubbles using qNano™ (Izon®, Christchurch, NZ). In this characterisation method the microbubbles solution is forced toward a nanopore, and when a microbubble passes the pore it causes a transient in the ionic current flow. A detailed description and critical evaluation of the TRPS technique and qNano™ can be found in [41,42].

Size and concentration calibrations were performed using a particle standard of known size and concentration as a reference. Polystyrene traceable particle standards from the National Institute of Standards and Technology NIST, with a nominal mean diameter of 903 nm, denoted as CPN900 (Thermofisher™, Massachusetts, US) were used for calibration. CPN900 were diluted in PBS at concentrations of $2x10^8$/ml and $5x10^7$/ml for TRPS measurements, using thermoplastic polyurethane nanopores. NP400, NP800 and NP2000 nanopores capable of sizing 185-1100 nm, 385-2050 nm and 935-5700 nm particles respectively were used in this study. Blockade counts pertinent for these experiments for calibration and samples typically ranged between 500 and 3000 events per measurement.

Microbubbles solutions were then diluted in PBS at a dilution ratio of 1:1000.Approximately 40 µL of the diluted solutions were loaded into top fluid cell of qNano™. Their concentrations were then determined using a single point pressure method [43], with the applied pressure ranging between 1-2 kPa. For the pore sizes (NP400, NP800, NP2000) and the pressures used in this study, convection is the most dominant particle transport mechanism (when compared with electrophoresis and electroosmosis) and hence a single point pressure as opposed to a more lengthy multiple point pressure method is sufficient to accurately calculate the concentration of the microbubbles. Each counting experiment was performed for three trials to account for measurement uncertainty.

Attenuation measurement setup

Dilutions of 1:2000 of Definity™ and 1:20 of the ELIP were prepared. The lower Liposomes dilution is due to the lower attenuation caused by them, because of their higher lipid to gas volume fraction, where lipids have an acoustic impedance that is close to the impedance of the PBS solution itself [44], and due to a portion of the liposomes population being non-echogenic as not all of them entrap gas.

The diluted microbubble samples were shaken by hand before filling a 12.25 mL test chamber. The test chamber was positioned in a water bath between an immersion transducer and a 0.2 mm diameter needle hydrophone (Precision acoustic®, Dorset, UK) as shown in Fig.1. The sample was circulating through the chamber using a peristaltic pump to avoid the possible risk of flotation. However, during excitation and data collection the fluid was observed to be stationary. The sample was changed with every transducer to account for possible sample degradation due to repeated excitation exposure. A set of immersion transducers V381 (3.5 MHz), V308 (5 MHz), V321 (7.5 MHz), A327 (10 MHz), V319 (15 MHz) and V317 (20 MHz) (Olympus®, Tokyo, JP) were used to cover a range of frequencies from 2-20 MHz, at 1 MHz intervals. The transducers were excited in burst mode at 50 cycles by 10 ms inter pulse period, using an arbitrary function generator DG4062 (Rigol®, Beijing, CN), and the signal of the acoustic wave after passing the bubbles chamber was acquired by the hydrophone powered by a DC coupler, using an oscilloscope MSO-5074 (Rigol®, Beijing, CN). Fast Fourier Transform was applied on the signal and the amplitude corresponding to the excitation frequency was recorded. The water bath was heated to 37±0.1 ˚C for the experiments performed at physiological temperature. The bubble solutions in crimp-capped vials were also heated to 37±0.1 ˚C, before filling the test chamber.

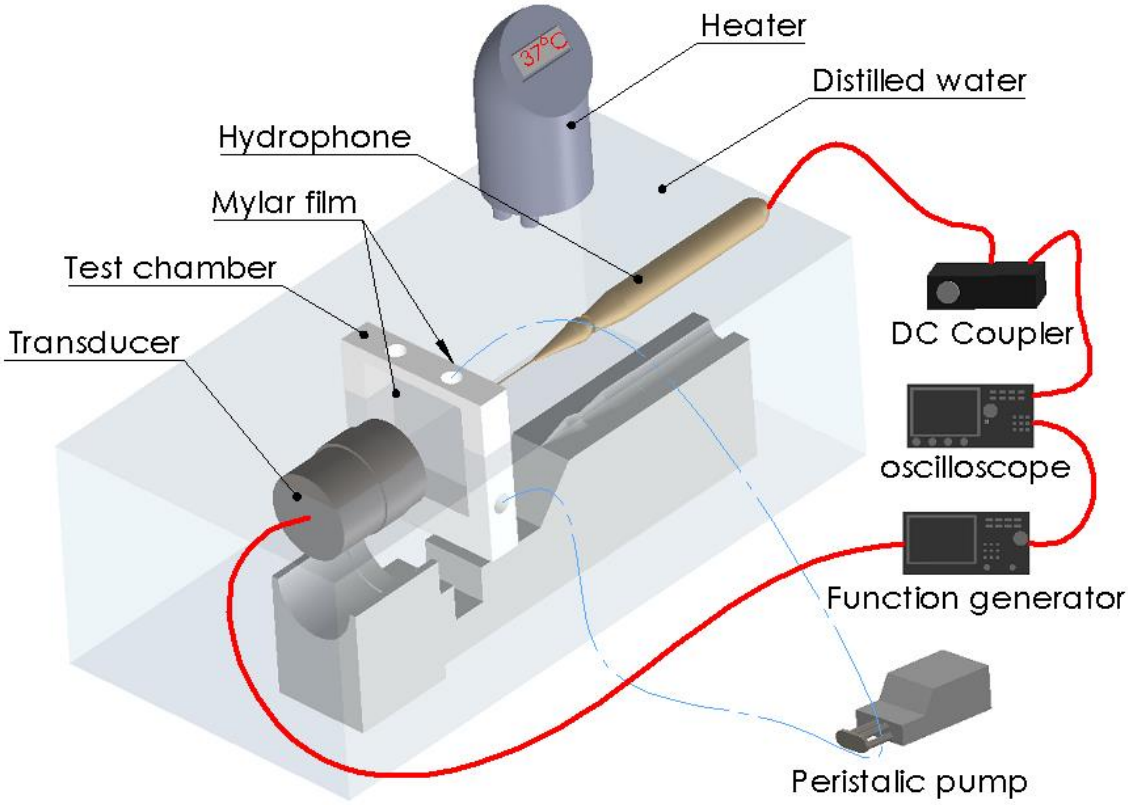

Figure 1: schematic of through transmission attenuation measurement experiment. The top of the test chamber is above the water surface.

The experimental attenuation coefficient α_{exp} was calculated, by relating the received pressure passing the test chamber filled with pure PBS solution P_i to the pressure through solutions with bubbles P_b using equation (9).

$$\alpha_{exp} = {20log_{10}\left(\frac{P_i}{P_b}\right)}/{L} \quad (9)$$

where L is the length of the path over which the acoustic wave interacts with the microbubbles. In this setup, it corresponds to the width of the test camber in Figure1 and it is 1 cm. The distance between the transducer and the test chamber is 1 cm and between the hydrophone and the test chamber is 0.1 cm. The lowest possible pressure that will result in detectible pressure levels after attenuation using this setup was found to be 11 kPa.

Constant excitation pressure

The required excitation voltages to produce an 11 kPa pressure wave inside the test chamber were measured at each frequency before performing the experiment. This is to eliminate pressure dependent attenuation effects discussed earlier. The hydrophone manufacturer's calibration data were used to calculate the received voltage corresponding to 11 kPa, and the transducer was excited with varying voltages until the desired received voltage was measured by the hydrophone. The transducers were then excited at those voltages (Fig.2a) five times to account for the uncertainty in the signal. According to (Fig.2 a) the 10 MHz transducer requires substantially lower voltages relative to the other transducers. This can be explained since the 10 MHz transducer is a low damping accuscan transducer whilst all the others are heavily damped videoscan transducers. Figure.2 b shows the pressure developed inside the chamber accounting for the uncertainty of calibration measurements and the 13% uncertainty reported by the hydrophone manufacturer in their calibration report. The legends in Figures 2a and 2b refer to the centre frequency of each transducer.

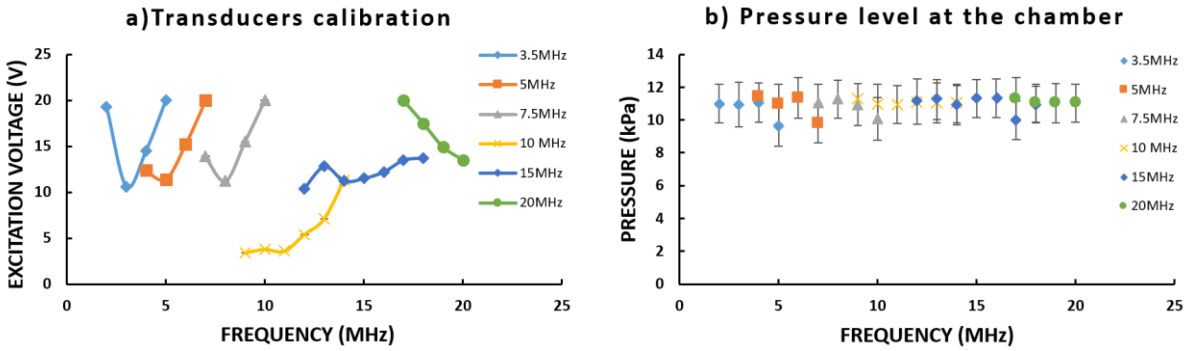

Figure 2: Transducers calibration data representing a) excitation voltages used to produce 11 kPa acoustic wave, b) Pressure readings inside the test chamber.

RESULTS

The shell properties, ultrasound images and size distribution of freshly prepared Definity™ and ELIP at room temperature and physiological temperature are presented, along with the results of the time dependent concentration and size distribution stability studies.

Ultrasonic imaging

Figure 3 shows the ultrasonic images of a 9 mm inner diameter syringe filled with PBS, Definity™ microbubbles and ELIP both at 1:500 dilution. ELIP showed lower echogenicity in comparison to Definity™ microbubbles under similar imaging parameters.

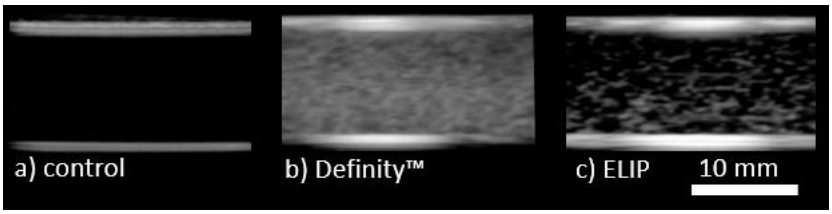

Figure 3: Ultrasonic imaging at 18 MHz and 0.26 MI of a) PBS, b) Definity™ and c) ELIP.

Size and concentration stability

Number distributions by diameter are presented for both Definity™ and ELIP in Figure 4. The distributions are corrected for dilution, thus the results shown represent the distribution in the original vials before dilution. Although, the results are acquired for individual bubble diameters, the bubbles are grouped in bins of 50 nm size variations for better visualisation. These distributions were used in Eq. (1) and Eq. (8) to calculate the best frequency dependent attenuation curves for microbubbles and ELIP respectively, and presented in the next section.

The summary of the volume weighted average diameters are presented in Table 2. The volume weighted mean diameters are reported for the sake of comparison with other studies. However, the change in the volume weighted diameters with temperature and time, might not be descriptive to the change in the population. The volume weighted mean diameter is affected more by larger diameter bubbles, and size distributions represented in Figure 4 show that the highest concentrations are at the smaller diameters of the measured range. Therefore, median diameters are also presented in Table 2, as the change in the median with respect to time and temperature is more descriptive to the change in the population.

The volume weighted mean diameters of both Definity™ and ELIP increased at physiological temperature in comparison to room temperature. The volume weighted average diameter of Definity™ increased from 983 nm to 1334 nm and the median from 632 nm to 675 nm when the temperature increased from 25 °C to 37 °C. Similarly, the ELIP volume weighted average diameter increased from 1184 nm to 1214 nm and the median from 710 nm to 732 nm when the temperature increased from 25 °C to 37 °C.

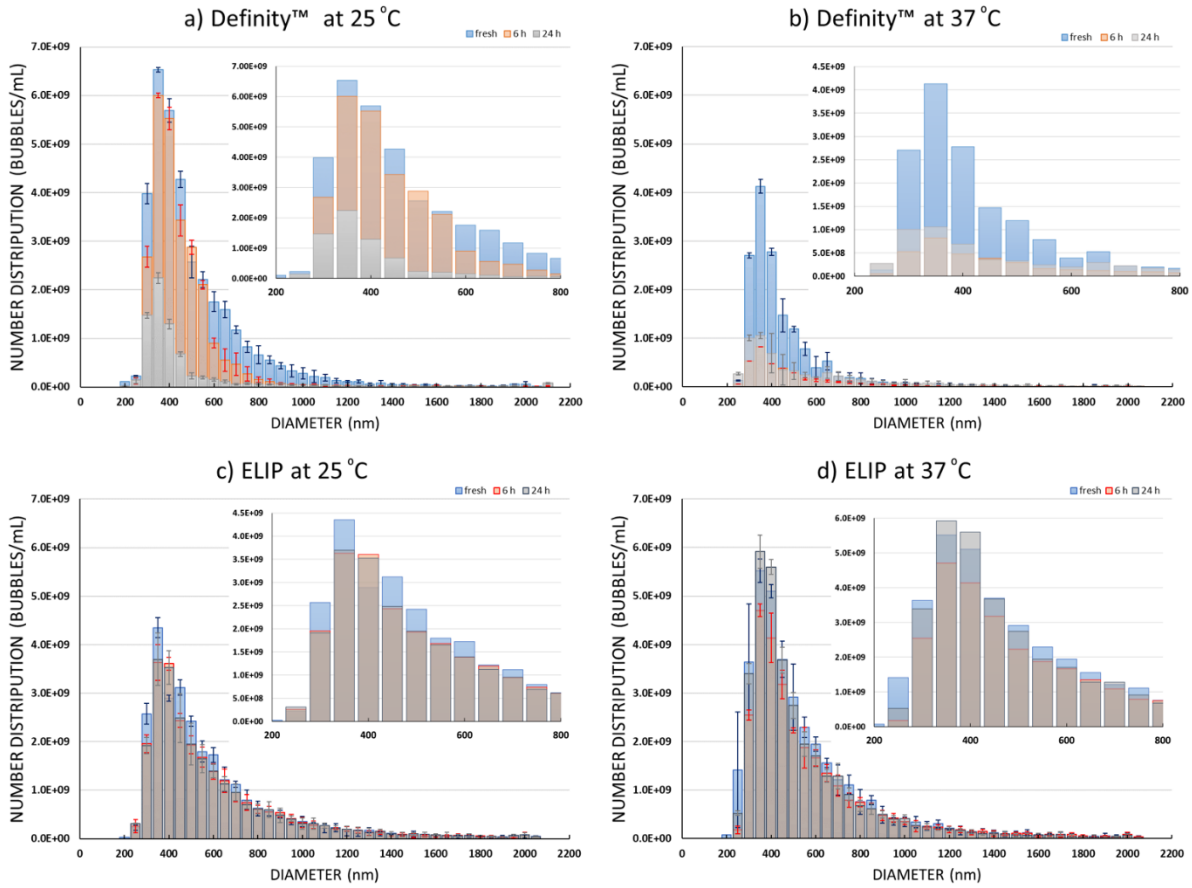

Figure 4:TRPS size distribution of a) Definity™ at 25 °C, b) Definity™ at 37 °C, c) ELIP at 25 °C, d) ELIP at 37 °C. The figures represent 200 nm to 2200 nm diameters for better representations of the data, as after 2200 nm diameter counts are minimal relative

The concentration of Definity™ at 25 °C declined significantly with time, losing 26% and 79% of the total concentration after 6 and 24 hours of activation, respectively (Fig.4.a). On the contrary, the ELIP lost 8% and 9% of their total concentration after 6 and 24 hours at the same temperature (Fig.4.c). Next, freshly prepared Definity™ were evaluated at body temperature i.e. 37 °C, and under these conditions the concentration decreased by 58% relative to the sample concentration at room temperature. After 24 hours at 37 °C, this loss increased to 73% of the concentration it had when first reaching physiological temperature, 24 hrs earlier. In the case of the ELIP their concentration increased after the temperature was raised to 37 °C. This unexpected result could be due to small microbubbles, which were below the detectable range at room temperature, expanding and then falling into the detectable range. ELIP then maintained > 80% of their concentration relative to their fresh concentration at 37 °C, over a period of 24 hours.

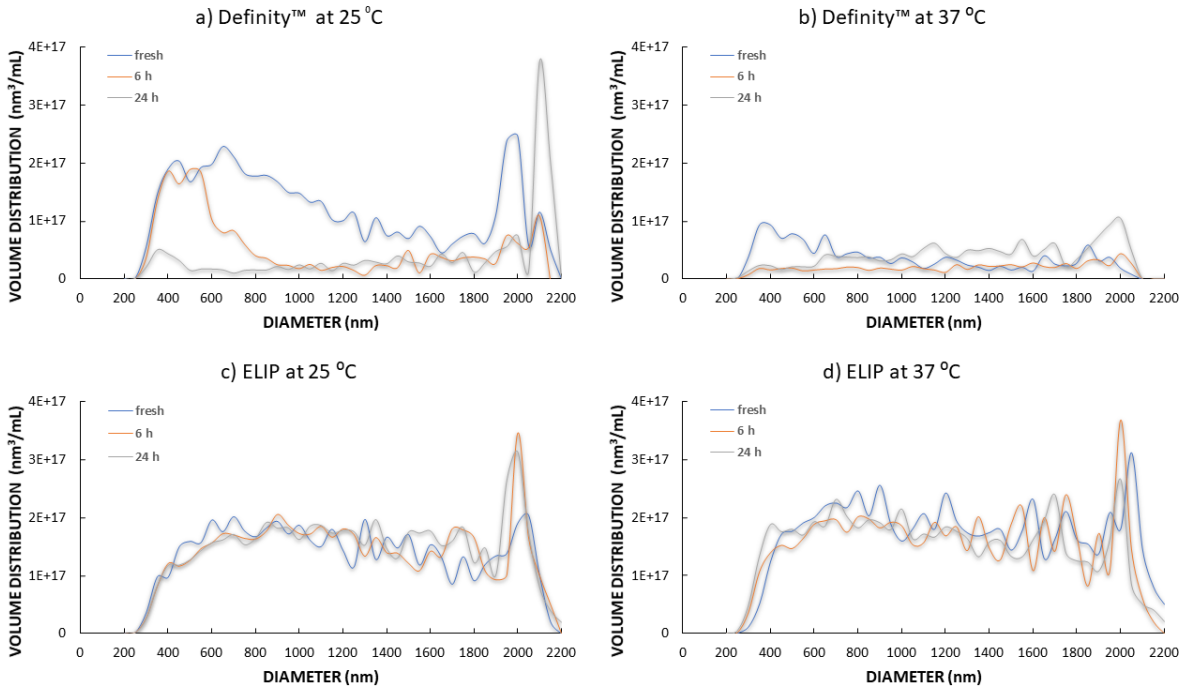

Figure 5: TRPS volume distribution of a) Definity™ at 25 °C, b) Definity™ at 37 °C, c) ELIP at 25 °C, d) ELIP at 37 °C.

The volume distributions are shown in Figure 5 and total volume fractions representing the volume occupied by the microbubbles in each millilitre of PBS solution are shown in Table 2. The trend of smaller volume fraction despite the increase of the concentration in the ELIP at 37 ˚C could be due to fragmentation of large bubbles into smaller bubbles as an increase in the number of smaller bubbles can be seen in Fig.4-d and consequently in volume distribution in Fig.5-d in comparison to Fig.4-c and Fig.5-c respectively .

Table 2: Summary of counting and sizing results

Agents	Mean vol. wgt. dia. (nm)			Median diameter (nm)			Total concentration $\times 10^{10}$ (μbubbles/mL)			Volume fraction $\times 10^{18}$ (nm³/mL)		
	Freshly prepared	6 h	24 h	Freshly prepared	6 h	24 h	Freshly prepared	6 h	24 h	Freshly prepared	6 h	24 h
Definity™ 25 °C	983±64	1047±71	1486±8	632±21	605±21	591±17	3.46	2.57	0.737	4.84	2.15	1.37
Definity™ 37 °C	1334±97	1601±63	1468±56	675±39	750±19	777±28	1.45	0.371	0.393	1.38	0.753	1.54
ELIP 25 °C	1184±21	1260±23	1285±20	710±12	691±20	687±15	2.67	2.45	2.44	5.39	5.48	5.82
ELIP 37 °C	1214±24	1245±22	1227±17	732±29	738±15	730±17	3.58	2.87	3.1	6.69	6.05	6.01

Frequency dependent attenuation and shell parameters

The frequency dependent attenuation curves of both microbubbles and liposome at room temperature and physiological temperature are presented in Figure 6. Definity™ show a shift of the peak magnitude in the attenuation curve towards lower frequency at physiological temperature compared to room temperature. The peak attenuation was 20.8 dB/cm at (10 MHz, 25 ºC) and 22.1 dB/cm at (9MHz, 37 ºC). For ELIP the peak attenuation was at 4 MHz at both temperatures.

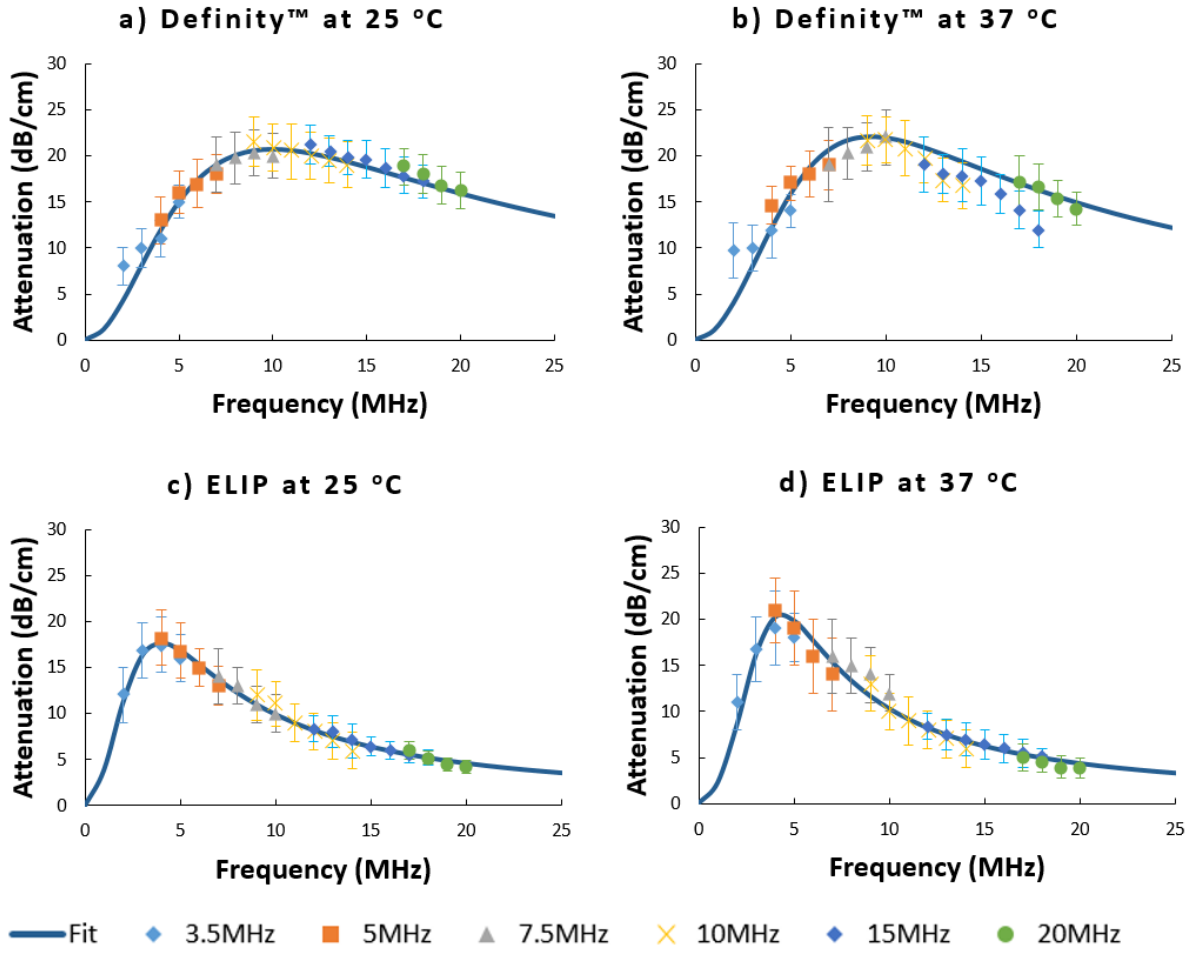

Figure 6: Frequency dependent attenuation curve of a) Definity™ at 25 ˚C, b) Definity™ at 37 ˚C, c) ELIP at 25 ˚C, d) ELIP at 37 ˚C. The legend below shows the transducer by their centre frequency.

Equation 1 was used for Definity™ and equation 8 for ELIP to determine the optimal values of the stiffness S_p and friction S_f coefficient to best fit the measured attenuation data by minimising the sum squared error as detailed in [45]. The estimated shell parameters are presented in Table-3. For ELIP the size distributions were normalized and substituted as n_k and the best fit of total number concentration N_{fit} was calculated to be 0.83×10^{10} and 6.8×10^{9} in comparison to the measured values 2.67×10^{10} and 3.58×10^{10} at 25 °C and 37 °C respectively.

Table 3: Summary of estimated shell parameters and r square value of the fitting curves

agents	25 ºC			37 ºC		
	$S_p(N/m)$	$S_f\ 10^{-6}\ (kg/s)$	R^2	$S_p(N/m)$	$S_f\ 10^{-6}\ (kg/s)$	R^2
Definity™	1.53±0.08	1.51±0.12	0.96	1.18±0.16	1.09±0.2	0.90
ELIP	0.11±0.02	0.31±0.03	0.97	0.15±0.01	0.29±0.01	0.99

DISCUSSION

The volume weighted mean of fresh Definity™ was found to be (1093 nm) using TRPS, in comparison to (3.99 µm) and (1.6 µm) measured using a coulter counter with 20 µm [21] and 30 µm [22] aperture tubes, respectively. This can be attributed to the large number of small-sized microbubbles having diameters below the minimum measurable limit of detection by the coulter counter. The minimum measurable diameter in these studies was 0.46 µm [21] and 0.6 µm [22]. However, the blue bins in (Fig.4, a) show that the largest concentrations measured by TRPS are below these minimums. Consequently, the concentrations of Definity™ microbubbles measured using

TRPS were significantly higher than those measured using coulter counter. The total concentration of the fresh Definity™ sample measured using TRPS was 3.46×10^{10} bubble/mL in comparison to 1.30×10^{10} bubble/mL [21] measured using the coulter counter technique. Definity™ MBs were shown to loss 26% and 79% of their fresh concentration after 6 and 24 hours of activation respectively, in comparison to 16% and 56 % of their fresh number concentration after 1 hour and 3 hours of activation respectively in that study [21].

The concentration measurements are for the total population of the ELIPs which includes echogenic liposomes estimated from the attenuation graph as N_{fit}, and non-echogenic liposomes. Therefore, the ELIPs maintaining their concentration for 24 hours does not imply they retained their entrapped gas, as liposomes could exist even if they lose their entrapped gas. However, in the case of monolayer MBs, the assumption of the whole population retaining gas is valid as monolayer MBs will only exist if they entrap a hydrophobic gas.

The median diameters of both microbubbles at 25 °C decreased with time as shown in Table 2. However, this does not necessarily mean that individual microbubbles are contracting. Considering the change of the concentration with time, large microbubbles could have burst. This is in disagreement with [21], where Definity™ MBs were shown to have a decreasing volume weighted mean diameter over time, from 3.99 µm 30 s after activation to 1.36 µm and 0.98 µm after 1 and 3 hours of activation respectively. The volume weighted mean diameter in the presented data was shown to increase from 983 nm right after activation to 1047 nm and 1486 after 6 and 24 hours of activation respectively. In general, ELIPs have shown lower radial dimensional changes with time in comparison to monolayer microbubbles. This is expected as they entrap less gas in comparison to the monolayer MBs, and because of the presence of a large number of liposomes in the ELIP sample that are non-echogenic as estimated from the fitting of the attenuation curve. The proportion of non-echogenic liposomes in the ELIP samples is ~69% and ~81% at 25 °C and 37 °C, respectively.

There are some limitations about the determination of thermal-radial change and time-radial change of polydisperse samples. Microbubbles below the detection threshold could have expanded and became detectable when the temperature increased. For future studies, thermal and time radial change of microbubbles could be investigated better using monodispersed microbubble populations, through size filtering. It is important to note that the number concentration stability measured in this study does not necessarily correlate with echogenicity. Some of the ELIP measured in the counting could have lost their gas but still be included in the concentration measurement.

The peak attenuation factor for the ELIP was 17.5 dB/cm at 25 °C and 20.1 dB/cm at 37 °C. The attenuation factor at physiological temperature was higher at the frequencies close to the peak and lower at the frequencies far from the peak relative to the attenuation at room temperature for both agents. Both agents were filled with octafluoropropane gas which has a very low solubility in aqueous medium [46], which enhance thermodynamic stability. Therefore, it is likely that the change in the frequency dependent attenuation with temperature is due to the change in the shell viscoelastic properties. Although Definity™ attenuation curves are in agreement with the previously published study[22], the estimated value of friction parameter varies significantly. The friction coefficient was estimated to be $1.51 \times 10^6 kg/s$ in comparison to $0.47 \times 10^6\ kg/s$ previously reported by [22]. This is mainly because of the different size distributions used in Eq. 1, where TRPS counting technique showed that there are large numbers of Definity™ microbubbles with diameters significantly smaller than coulter counter measurement limits, as mentioned previously. However the values of the stiffness at both physiological and room temperatures were in agreement with the previously published studies. The stiffness of Definity™ microbubbles was found to be (1.53 N/m at 25 ºC) in comparisons to (1.76 N/m at 25 ºC) at both[30,22] and (1.18 N/m at 37 ºC) in comparisons to (1.01 N/m at 37 ºC) in [30] and (1.10 N/m at 37 ºC) in [22].

The ELIP were shown to have a very low rigidity where the stiffness coefficient was found to be 0.11 N/m. This could partially be due to the nature of the lipid blind used to formulate the shell. An Atomic Force Microscopy investigation found that the presence of charged lipids reduces their stiffness by 30%-60% in comparison to those formulated of neutrally charged lipids [47]. Thus, the low rigidity could be due to the presence of DSPE lipid which has a -1 net surface charge at 7.4 pH. Despite their low rigidity, the nano-size ELIP were shown to retain their echogenicity for eight weeks [8]. This implies, they maintain the gas within them, as the gas acoustic

impedance difference compared to the impedance of the surrounding aqueous medium is the cause of echogenicity. Another Atomic Force Microscopy investigation found that the stiffness of liposomes made of DSPC:DSPE-PEG2000:DSPE-PEG2000-C at a molar ratio of 90:5:5 between 0.004 and 0.22 N/m [48]. Although the formulation is different, the study gives an insight of the stiffness of liposomes.

The trend of decreased rigidity of Definity™ and increased rigidity of ELIP as temperature increased is in agreement with previously published studies (Table.1) where Definity™ was shown to have lower stiffness at physiological temperature in comparison to room temperature, and three different formulations of echogenic liposomes ELIP were shown to have higher stiffness at physiological temperature compared to their stiffness at room temperature [22]. The stiffness increased from 1.13 N/m at 25ºC to 1.49 N/m at 37ºC for ELIPs made of L-α-phosphatidylcholine (EggPC), 1,2-dipalmitoyl-*sn*-glycero-3-phosphoethanolamine (DPPE), 1,2-dipalmitoyl-*sn*-glycero-3-phospho-[1′-rac-glycerol] (DPPG) and cholesterol (CH) at a molar ratio of 69:8:8:15, from 1.98 N/m at 25 ºC to 3.10 N/m at 37 ºC for ELIPs made of EggPC:DPPC:DPPE:DPPG:CH at a molar ratio of 27:42:8:8:15, and from 2.05 N/m at 25 ºC to 4.06 N/m at 37 ºC for ELIPs made of DPPC:DOPC:DPPG:CH at a molar ratio of 46:24:24:6.

As discussed in the critical aspects of experimental procedures, the results presented for the shell parameters in this study are an average representative of the MBs and ELIPs population and do not necessarily represent individual bubbles. The method derives the mechanical properties of a single bubble from a polydisperse sample, where frequency and size dependant effects are inevitable. The accuracy of the measurements could be improved by performing the experiments on monodisperse samples as in [36,49]. However estimating the average parameters of the native polydisperse population is important for future acoustofluidic manipulation studies as maintaining monodispersity of MBs for long time is challenging[50]. Another limitation of the attenuation experiments was the long attenuation path (1 cm), which could have affected attenuation measurements due to the multiple interaction between the acoustic wave and large number of bubbles and the reflected waves from the bubbles. Future measurements should reduce such effects through reducing concentration and the length of the attenuation path.

CONCLUSION

The investigation of the microbubbles and liposome stiffness and stability properties at room and physiological temperature shows that the new formulation of ELIP have an extended number-concentration and size stability profile relative to the monolayer microbubble Definity™. The acoustofluidic delivery agent displayed lower thermal radial changes relative to the monolayer ultrasound contrast agent, and underwent lower radial expansion over time. The ELIP shell parameters estimated in this study show a very low stiffness coefficient and friction coefficient relative to the monolayer microbubble. The size measurements showed that most of Definity™ population are sub-micron size where half of the population have diameters below 632 nm, unlike what was reported in previous studies and claimed by the manufacturer.

Future research on the translation velocity caused by sonication of the new acoustofluidic delivery agent is ongoing based on the shell parameter estimation of the agents. Further research to validate their shell stiffness estimated in this study, could include atomic force microscopy mechanical loading. Resonance mass measurement could also be used to distinguish the ELIP from non-echogenic liposomes to further enhance the accuracy of frequency attenuation dependent studies on characterising ELIP.

ACKNOWLEDGMENT

The authors thank Mr. Jarrad Humphry and Mr. Alessandro Carcione for providing technical assistance and thoughtful discussions. The authors are also grateful for the support of The Saudi Arabia Cultural mission for supporting the first author in the form of a scholarship.

RESOURCES

1. Cosgrove D (2006) Ultrasound contrast agents: an overview. European journal of radiology 60 (3):324-330
2. Quaia E (2007) Microbubble ultrasound contrast agents: an update. European radiology 17 (8):1995-2008
3. Hoff L (2001) Acoustic characterization of contrast agents for medical ultrasound imaging. Springer Science & Business Media,
4. Paul S, Nahire R, Mallik S, Sarkar K (2014) Encapsulated microbubbles and echogenic liposomes for contrast ultrasound imaging and targeted drug delivery. Computational mechanics 53 (3):413-435
5. Fan C-H, Ting C-Y, Liu H-L, Huang C-Y, Hsieh H-Y, Yen T-C, Wei K-C, Yeh C-K (2013) Antiangiogenic-targeting drug-loaded microbubbles combined with focused ultrasound for glioma treatment. Biomaterials 34 (8):2142-2155
6. Ferrara K, Pollard R, Borden M (2007) Ultrasound microbubble contrast agents: fundamentals and application to gene and drug delivery. Annu Rev Biomed Eng 9:415-447
7. Feinstein SB, Coll B, Staub D, Adam D, Schinkel AF, Folkert J, Thomenius K (2010) Contrast enhanced ultrasound imaging. Journal of nuclear cardiology 17 (1):106-115
8. Thakur SS, Ward MS, Popat A, Flemming NB, Parat M-O, Barnett NL, Parekh HS (2017) Stably engineered nanobubbles and ultrasound-An effective platform for enhanced macromolecular delivery to representative cells of the retina. PloS one 12 (5):e0178305
9. Bekeredjian R, Grayburn PA, Shohet RV (2005) Use of ultrasound contrast agents for gene or drug delivery in cardiovascular medicine. Journal of the American College of Cardiology 45 (3):329-335
10. Mitragotri S (2005) Healing sound: the use of ultrasound in drug delivery and other therapeutic applications. Nature reviews Drug discovery 4 (3):255
11. Qiu Y, Zhang C, Tu J, Zhang D (2012) Microbubble-induced sonoporation involved in ultrasound-mediated DNA transfection in vitro at low acoustic pressures. Journal of biomechanics 45 (8):1339-1345
12. Lea-Banks H, Teo B, Stride E, Coussios CC (2016) The effect of particle density on ultrasound-mediated transport of nanoparticles. Physics in Medicine & Biology 61 (22):7906
13. Pislaru SV, Pislaru C, Kinnick RR, Singh R, Gulati R, Greenleaf JF, Simari RD (2003) Optimization of ultrasound-mediated gene transfer: comparison of contrast agents and ultrasound modalities. European heart journal 24 (18):1690-1698
14. Unger EC, Matsunaga TO, McCreery T, Schumann P, Sweitzer R, Quigley R (2002) Therapeutic applications of microbubbles. European journal of Radiology 42 (2):160-168
15. Frenkel PA, Chen S, Thai T, Shohet RV, Grayburn PA (2002) DNA-loaded albumin microbubbles enhance ultrasound-mediated transfection in vitro. Ultrasound in medicine & biology 28 (6):817-822
16. PAREKH H, THAKUR S (2018) Method for Preparing a Lipid Bubble. Australia Patent WO/2018/053601,
17. Thakur SS, Chen Y-S, Houston ZH, Fletcher N, Barnett NL, Thurecht KJ, Rupenthal ID, Parekh HS (2019) Ultrasound-responsive nanobubbles for enhanced intravitreal drug migration: An ex vivo evaluation. European Journal of Pharmaceutics and Biopharmaceutics 136:102-107
18. Alsadiq H, Tupally K, Kokil G, Vogel R, Parekh H, Veidt M (2019) Concentration stability of monolayer and bilayer lipid microbubbles–a precursor for new drug delivery applications.
19. Vogel R, Pal AK, Jambhrunkar S, Patel P, Thakur SS, Reátegui E, Parekh HS, Saá P, Stassinopoulos A, Broom MF (2017) High-resolution single particle zeta potential characterisation of biological nanoparticles using tunable resistive pulse sensing. Scientific reports 7 (1):17479
20. Kotopoulis S, Postema M (2010) Microfoam formation in a capillary. Ultrasonics 50 (2):260-268
21. Goertz DE, de Jong N, van der Steen AFJUim, biology (2007) Attenuation and size distribution measurements of Definity™ and manipulated Definity™ populations. 33 (9):1376-1388

22. Raymond JL, Haworth KJ, Bader KB, Radhakrishnan K, Griffin JK, Huang S-L, McPherson DD, Holland CK (2014) Broadband attenuation measurements of phospholipid-shelled ultrasound contrast agents. Ultrasound in medicine & biology 40 (2):410-421
23. Gorce J-M, Arditi M, Schneider M (2000) Influence of bubble size distribution on the echogenicity of ultrasound contrast agents: A study of SonoVue™. Investigative radiology 35 (11):661-671
24. Medwin H (1977) Counting bubbles acoustically: a review. Ultrasonics 15 (1):7-13
25. de Jong N, Hoff L, Skotland T, Bom N (1992) Absorption and scatter of encapsulated gas filled microspheres: theoretical considerations and some measurements. Ultrasonics 30 (2):95-103
26. Faez T, Goertz D, De Jong N (2011) Characterization of Definity™ ultrasound contrast agent at frequency range of 5–15 MHz. Ultrasound in medicine & biology 37 (2):338-342
27. Sun Y, Kruse DE, Dayton PA, Ferrara KW (2005) High-frequency dynamics of ultrasound contrast agents. IEEE transactions on ultrasonics, ferroelectrics, and frequency control 52 (11):1981-1991
28. Bloch SH, Wan M, Dayton PA, Ferrara KW (2004) Optical observation of lipid-and polymer-shelled ultrasound microbubble contrast agents. Applied physics letters 84 (4):631-633
29. Faez T, Goertz D, De Jong N (2011) Characterization of Definity™ ultrasound contrast agent at frequency range of 5–15 MHz. Ultrasound in medicine and biology 37 (2):338-342
30. Shekhar H, Smith NJ, Raymond JL, Holland CK (2018) Effect of temperature on the size distribution, shell properties, and stability of Definity®. Ultrasound in medicine & biology 44 (2):434-446
31. Chen Q, Zagzebski J, Wilson T, Stiles T (2002) Pressure-dependent attenuation in ultrasound contrast agents. Ultrasound in medicine & biology 28 (8):1041-1051
32. Tang M-X, Eckersley RJ, Noble JA (2005) Pressure-dependent attenuation with microbubbles at low mechanical index. Ultrasound in medicine & biology 31 (3):377-384
33. Tang M-X, Eckersley RJ (2007) Frequency and pressure dependent attenuation and scattering by microbubbles. Ultrasound in medicine & biology 33 (1):164-168
34. Helfield BL, Goertz DE (2013) Nonlinear resonance behavior and linear shell estimates for Definity™ and MicroMarker™ assessed with acoustic microbubble spectroscopy. The Journal of the Acoustical Society of America 133 (2):1158-1168
35. Overvelde M, Garbin V, Sijl J, Dollet B, De Jong N, Lohse D, Versluis MJUim, biology (2010) Nonlinear shell behavior of phospholipid-coated microbubbles. 36 (12):2080-2092
36. Segers T, de Jong N, Versluis MJTJotASoA (2016) Uniform scattering and attenuation of acoustically sorted ultrasound contrast agents: Modeling and experiments. 140 (4):2506-2517
37. Segers T, Gaud E, Versluis M, Frinking PJSm (2018) High-precision acoustic measurements of the nonlinear dilatational elasticity of phospholipid coated monodisperse microbubbles. 14 (47):9550-9561
38. Acconcia CN, Wright A, Goertz DE (2018) Translational dynamics of individual microbubbles with millisecond scale ultrasound pulses. The Journal of the Acoustical Society of America 144 (5):2859-2870
39. Alsadiq H, Reddy K, Parekh H, Veidt M Influence of acoustofluidic parameters on velocity streaming of sonicated medical microbubbles. In: Proceedings of ACOUSTICS, 2018. vol 9.
40. Definity Safety Label FDA/Center for Drug Evaluation and Research (Octoper 2011). Silver Spring, MD, USA
41. Willmott G, Vogel R, Yu S, Groenewegen L, Roberts G, Kozak D, Anderson W, Trau M (2010) Use of tunable nanopore blockade rates to investigate colloidal dispersions. Journal of Physics: Condensed Matter 22 (45):454116
42. Vogel R, Willmott G, Kozak D, Roberts GS, Anderson W, Groenewegen L, Glossop B, Barnett A, Turner A, Trau M (2011) Quantitative sizing of nano/microparticles with a tunable elastomeric pore sensor. Analytical chemistry 83 (9):3499-3506
43. Roberts GS, Yu S, Zeng Q, Chan LC, Anderson W, Colby AH, Grinstaff MW, Reid S, Vogel R (2012) Tunable pores for measuring concentrations of synthetic and biological nanoparticle dispersions. Biosensors and Bioelectronics 31 (1):17-25

44. Varanasi U, Apfel RE, Malins DC (1977) A novel microtechnique for the measurement of acoustic properties of lipids. Chemistry and Physics of Lipids 19 (2):179-184
45. Hoff L, Sontum PC, Hovem JM (2000) Oscillations of polymeric microbubbles: Effect of the encapsulating shell. The Journal of the Acoustical Society of America 107 (4):2272-2280
46. Yalkowsky SH, Dannenfelser RMJCoP, University of Arizona, Tucson, AZ (1992) Aquasol database of aqueous solubility. 189
47. Takechi-Haraya Y, Goda Y, Sakai-Kato K (2018) Atomic force microscopy study on the stiffness of nanosized liposomes containing charged lipids. Langmuir 34 (26):7805-7812
48. Chen CC, Wu S-Y, Finan JD, Morrison B, Konofagou EE (2013) An experimental study on the stiffness of size-isolated microbubbles using atomic force microscopy. IEEE transactions on ultrasonics, ferroelectrics, and frequency control 60 (3):524-534
49. Parrales MA, Fernandez JM, Perez-Saborid M, Kopechek JA, Porter TMJTJotASoA (2014) Acoustic characterization of monodisperse lipid-coated microbubbles: Relationship between size and shell viscoelastic properties. 136 (3):1077-1084
50. Talu E, Hettiarachchi K, Powell RL, Lee AP, Dayton PA, Longo MLJL (2008) Maintaining monodispersity in a microbubble population formed by flow-focusing. 24 (5):1745-1749